IET Renewable Power Generation

Special Issue Call for Papers

Be Seen. Be Cited.
Submit your work to a new IET special issue

Connect with researchers and experts in your field and share knowledge.

Be part of the latest research trends, faster.

Read more

The Institution of Engineering and Technology

Received: 10 February 2021 | Revised: 9 May 2021 | Accepted: 10 May 2021

DOI: 10.1049/rpg2.12213

IET Renewable Power Generation

The Institution of Engineering and Technology WILEY

ORIGINAL RESEARCH PAPER

Maximum power point tracking control for mechanical rectification wave energy converter

Jianan Xu | **Yanpeng Zhao** | **Yong Zhan** | **Yansong Yang**

College of Mechanical and Electrical Engineering, Harbin Engineering University, Harbin, Heilongjiang, China

Correspondence
College of Mechanical and Electrical Engineering, Harbin Engineering University, Harbin 150001, Heilongjiang Province, China.
Email: xujianan@hrbeu.edu.cn

Funding Information
The authors gratefully acknowledge the financial support from the Opening Fund of Acoustics Science and Technology Laboratory (Grant No. SSKF2020009).

Abstract

As a clean and renewable energy, wave energy has abundant reserves, and its reasonable development and utilization can effectively alleviate the problems of energy shortage and environmental pollution. This paper proposes a mechanical rectification wave energy converter. The reciprocating linear motion of the buoy is directly converted into the rotary motion through the ball screw. The magnetic coupling force transmission system is adopted to ensure the sealing of the device. Using mechanical rectification mechanism to ensure the service life of the generator. In addition, a dynamic model of the mechanical rectification wave energy converter is established. Through simulation analysis, the curve of power with load resistance is obtained. And there is an optimal load resistance value corresponding to the maximum power in different wave conditions. In order to improve the power generation efficiency, the maximum power point tracking control algorithm is designed based on the admittance differentiation method. By controlling the duty cycle of the switch tube in the Buck-Boost chopper circuit, the variable load is realized, and then the maximum power point tracking control is realized. Finally, simulation analysis verifies the feasibility of the algorithm under different wave conditions.

1 | INTRODUCTION

Energy is the material basis for human existence. With the development of science and technology and social economy, people's demand for energy is gradually increasing. However, traditional fossil fuels, such as coal, oil, and natural gas, have limited reserves, and large-scale use will cause environmental pollution problems [1]. As a kind of renewable energy, wave energy has abundant reserves, high energy density, and the installation of Wave Energy Converter (WEC) have little impact on the environment [2]. Therefore, the development and utilization of wave energy has great significance.

Generally, all of the WEC need a power take off system to convert the wave energy absorbed by the buoy into electrical energy. And PTO can be classified into hydraulic system, air turbine, hydro turbine, direct mechanical drive system and linear electrical generator [3–9]. Among them, hydraulic system and air turbine are relatively complicated in structure and difficult to maintain. The technology of hydro turbine is relatively mature, but its requirements for terrain are relatively high, while linear electrical generator usually requires larger size and higher cost. Therefore, this paper combines the WEC in [10, 11] to design a mechanical rectification WEC with a magnetic coupling force transmission system.

The WEC uses a ball screw as the energy conversion, which converts the low-speed linear motion of the buoy under the action of waves into high-speed rotating motion and transmits it to the generator. Besides, it uses a magnetic coupling force transmission system composed of neodymium iron boron permanent magnets. The buoy is directly coupled to the screw nut, which solves the problem of dynamic sealing when the buoy and the screw nut are connected in a marine environment. In addition, a mechanical rectification mechanism consisting of four bevel gears and two one-way clutches is added between the ball screw and the generator shaft, which rectifies the bidirectional rotational motion output by the ball screw and transmits it to the generator for continuous unidirectional rotational motion. The unidirectional rotating movement solves the problem of the generator's forward and reverse rotation and ensures the service life of the generator.

The actual marine environment is unpredictable, and there is a maximum power generation under different wave conditions. Therefore, we need to adopt some control strategies to find the maximum power under different wave conditions to improve power generation efficiency. Currently, there are many control methods for wave energy converter, such as the complex-conjugate control, latching control, model predictive control and maximum power point tracking control [12–19]. At present, complex-conjugate control is a theoretical control strategy, and it cannot be applied to the actual control system. In addition, latching control and model predictive control need to predict the incident waves. However, the actual wave conditions are difficult to accurately predict, so they are also difficult to implement. The maximum power point tracking control is a well-known adaptive control strategy that has achieved great success in other renewable energy industries (mainly solar and wind) [20, 21]. And there are relatively few applications in the field of wave energy.

Perturbation and observation method is currently the most widely used method for maximum power point tracking control. The output power at the current moment is calculated by sampling the output voltage and current. Then add a disturbance and compare it with the output power of the previous control period. If the power after the disturbance increases, the current disturbance direction is maintained, otherwise, the disturbance direction is changed. Its disadvantage is that there will be an oscillation error near the maximum power point, and the selection of its step size cannot take into account the tracking accuracy and response speed of the algorithm. The admittance differentiation method is an improvement of the disturbance observation method. The main improvement lies in setting the step length to a value proportional to the slope of the power curve. And it can reduce the oscillation error near the maximum power point and improving the tracking accuracy.

In this paper, the maximum power point tracking algorithm is designed based on the admittance differentiation method. By controlling the duty cycle of the circuit switch tube of the power generation system, the variable load regulation is realized, and then the maximum power is reached. Additionally, two low-pass filters are used to filter the average output power to make it more stable and improve the control accuracy of the algorithm under random wave conditions.

2 | DESIGN OF THE WEC

The overall structure of the mechanical rectification wave energy converter designed in this paper is shown in Figure 1. The WEC adopts mechanical direct drive PTO, avoiding the use of hydraulic system or air turbine and other intermediate converter, and the structure is simple and reliable.

The WEC mainly includes three parts: buoy, Mechanical Direct Drive PTO and generator. The buoy is mainly used to convert the absorbed wave energy into kinetic energy and transfer it to the PTO system. The diameter of the buoy is 1 m and the height is 0.2 m. As the key component of the WEC, the PTO system mainly transmits the wave energy absorbed by the buoy to the generator. The PTO system of the WEC designed in this paper mainly includes a ball screw and a mechanical rectification mechanism. Among them, the ball screw converts the vertical reciprocating linear motion of the buoy into the bidirectional rotational motion of the ball screw output shaft, and the mechanical rectifier mechanism converts the bidirectional rotational motion into continuous unidirectional rotational motion and transmits it to the generator. And then convert wave energy into electrical energy.

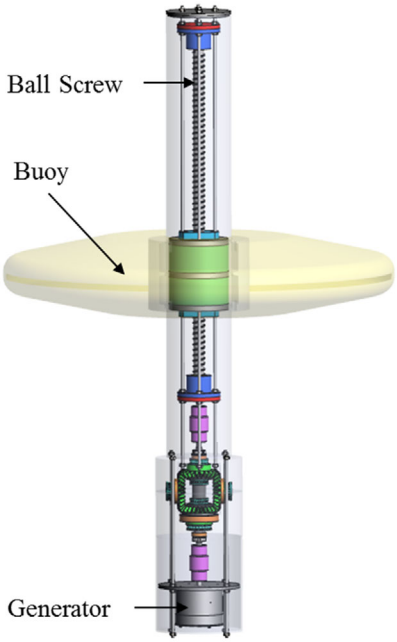

FIGURE 1 The overall structure of the wave energy converter

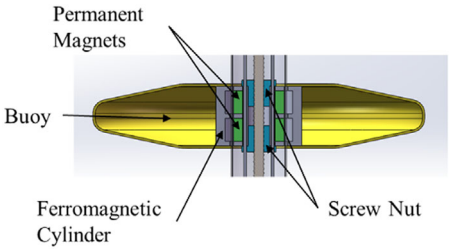

FIGURE 2 The structure of the magnetic coupling force transmission system

Due to the WEC works in a marine environment, in order to ensure its tightness, a magnetic coupling force transmission system is used between the buoy and the PTO system. As shown in Figure 2, a ring-shaped ferromagnetic cylinder is installed inside the buoy, and a ring-shaped neodymium-iron-boron permanent magnet is fixed on the ball screw nut. When the ferromagnetic cylinder in the buoy moves axially under the action of waves, it will interact with the screw nut. There will be magnetic resistance between the permanent magnets, which tends to restore the ferromagnetic cylinder to the position of minimum magnetic energy. Therefore, when the buoy moves upwards, the lead screw nut will move upwards together with the buoy, so that

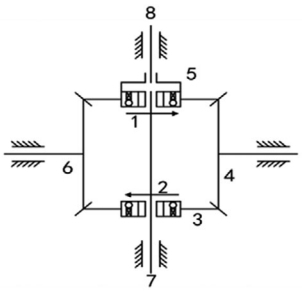

FIGURE 3 The diagram of the mechanical rectifier mechanism

the reciprocating linear motion of the buoy is transmitted to the lead screw nut, and converted into rotational motion through the ball screw. Since there is no physical contact between the buoy and the PTO system, the PTO system is in a completely sealed state, and when the device is overloaded under extreme weather conditions, the internal power generation system will not be damaged.

When the buoy makes reciprocating linear motion under the wave, the output of the ball screw is bidirectional rotary motion, which will affect the service life of the generator after being directly transmitted to the generator. Therefore, a mechanical rectification mechanism is added between the ball screw and the generator to convert the bidirectional rotary motion output by the ball screw into continuous unidirectional rotary motion and transmit it to the generator, thereby ensuring the service life of the generator.

Figure 3 is a schematic diagram of the mechanical rectifier. 1, 2 are two one-way clutches with opposite rotation directions, 3, 4, 5, and 6 are four bevel gears, 7 is the input shaft, and 8 is the output shaft. When the buoy moves upward, assuming the input shaft rotation direction is clockwise, the bottom one-way clutch is disengaged, the top one-way clutch is engaged, and the input movement is directly transmitted to the output shaft. When the buoy moves downwards, the rotation direction of the input shaft is counter clockwise. At this time, the bottom one-way clutch is engaged, and the top one-way clutch is disengaged. The input counter clockwise rotation direction is reversed to clockwise output by the action of four bevel gears. Through the mechanical rectification mechanism, the generator always rotates continuously in one direction, ensuring the service life of the generator.

3 | MODELING AND ANALYSIS OF THE WEC

3.1 | Hydrodynamic analysis of the buoy

The first step in designing WEC is to determine the wave force on the buoy. When the WEC is working, the buoy makes a vertical reciprocating linear motion under the wave. According to the linear wave theory [22], the hydrodynamic force of the buoy is the linear superposition of the Froude–Krylov force, the diffraction force and the radiation force. The Froude–Krylov force and the diffraction force are collectively called the wave excitation force, as shown in Equation (1).

$$F_e(\omega) = F_{FK}(\omega) + F_d(\omega) \tag{1}$$

where $F_e(\omega)$ is the wave excitation force, $F_{FK}(\omega)$ is the Frud-Krylov force, $F_d(\omega)$ is the diffraction force, ω is the wave frequency.

The radiation force generated by the movement of the buoy can be decomposed into additional mass force and radiation damping force, as shown in Equation (2).

$$F_r(\omega) = -\left(-\omega^2 m_a(\omega) + j\omega c_r(\omega)\right) z(\omega) \tag{2}$$

where $F_r(\omega)$ is the radiation damping force, $m_a(\omega)$ is the add mass, $c_r(\omega)$ is the radiation damping coefficient, $z(\omega)$ is the heave motion of buoy, j is the imaginary unit.

The hydrostatic restoring force is a force trying to return the structure to hydrostatic equilibrium, as shown in Equation (3).

$$F_h(\omega) = -\rho g A z(\omega) \tag{3}$$

where, $F_h(\omega)$ is the hydrostatic restoring force, ρ is the density of water, g is the acceleration of gravity, A is the cross-sectional area of the wetted surface.

From Equations (1)–(3), the total wave force acting on the buoy can be shown in Equation (4).

$$F_w = F_{FK}(\omega) + F_d + \omega^2 m_a(\omega) z(\omega) - j\omega c_r(\omega) z(\omega) - \rho g A z(\omega) \tag{4}$$

From the above analysis, it can be seen that the calculation of wave excitation force, additional mass, radiation damping and other hydrodynamic parameters is an important step in the analysis of the PTO system. This paper use the Hydrodynamic Diffraction module in ANSYS/ AQWA to calculate the hydrodynamic parameters.

According to the gravity centre position, moment of inertia and mass parameters calculated by SolidWorks software, the hydrodynamic solution analysis was carried out by AQWA. The amplitude of wave excitation force, additional mass, radiation damping, and Response Amplitude Operators (RAOs) of the buoy are obtained as shown in Figure 4.

It can be seen from the Figure 4 that when the wave period is 4 s, the wave excitation force of the buoy is 9810.25 N m^{-1}, the radiation damping is 191.77 N/(m/s), and the additional mass is 552.7 kg. By solving the hydrodynamic parameters of the buoy, it lays a foundation for the dynamic modelling and analysis of the WEC.

3.2 | Modelling of the PTO system

When the WEC is working, it is not only subjected to wave force, but also PTO force. Performing the inverse Fourierx

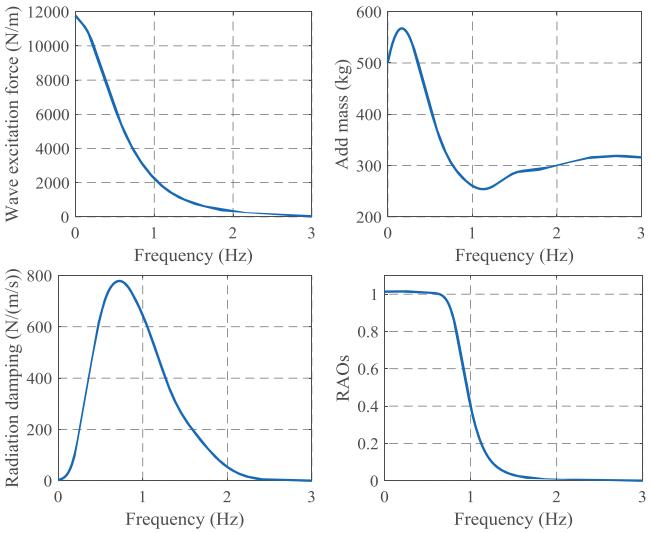

FIGURE 4 The amplitude of wave excitation force, add mass, radiation damping and RAOs

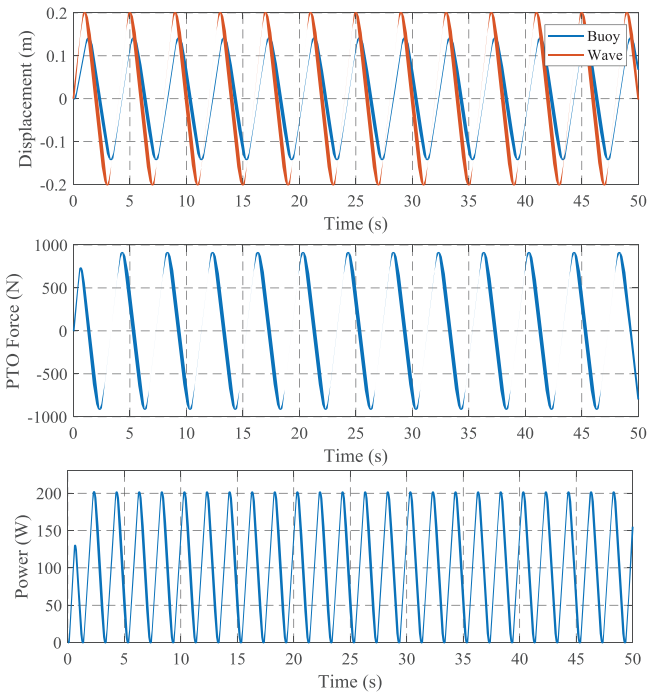

FIGURE 5 Wave and WEC displacement, PTO force and PTO power for linear PTO characteristics $C = 4000$ N/(m/s)

transform of Equation (4) and adding the PTO force can obtain the motion equation of the buoy as shown in Equation (5).

$$(m + m_{at})\,\ddot{z}(t) + c_{rt}\,\dot{z}(t) + \rho g A z\ (t) = F_{et} + F_{PTO} \tag{5}$$

According to Falnes's linear PTO theory [22], the linearized PTO system can be equivalent to a spring mass damping system, and the PTO force is resistance to the movement of the buoy, so the PTO force can be expressed as shown in Equation (6).

$$F_{PTO} = -m_p\ddot{z} - c_p\dot{z} - k_p z \tag{6}$$

Substituting Equation (6) into Equation (5) can get the motion equation of the buoy as shown in Equation (7).

$$\left(m + m_{at} + m_p\right)\ddot{z}(t) + \left(c_{rt} + c_p\right)\dot{z}(t) + \left(\rho g A + k_p\right) z\ (t) = F_{et} \tag{7}$$

The power generated with the linear PTO system is related to the equivalent damping coefficient, and the generated power can be calculated with Equation (8) [22].

$$P = c_p\,\dot{z}^2 \tag{8}$$

According to the calculated hydrodynamic parameter results, the motion response of the buoy when the damping coefficient is 4000 N/(m/s) can be calculated through MATLAB/Simulink software, and the result is shown in Figure 5. After the system is stabilized, the displacement amplitude of the buoy is 0.13 m, the peak PTO force is 910 N, the peak power of the PTO system is 204 W, and the average power is about 100 W.

The ball screw can realize the mutual conversion of rotary motion and linear motion. The internal ball rolling friction resistance is small and the transmission efficiency is high. In this paper, the ball screw is used to convert the low-speed reciprocating linear motion of the buoy into the high-speed rotational movement of the generator. The relationship between the axial force and torque can be expressed as shown in Equation (9).

$$F_s = \frac{2\pi}{l\eta_s}\,T_s \tag{9}$$

where, F_s is the axial force of the ball screw, l is the lead, η_s is the transmission efficiency, and T_s is the torque of the ball screw output shaft.

The motion equation of the ball screw can be expressed as shown in Equation (10).

$$\theta_s = \frac{2\pi}{l}\,z \tag{10}$$

where, θ_s is the rotation angle of the screw shaft and z is the axial displacement of the screw nut.

The angular velocity of the screw can be expressed as shown in Equation (11).

$$\omega_s = \frac{2\pi}{l}\,v \tag{11}$$

where, ω_s is the rotational angular velocity of the screw shaft and v is the axial velocity of the screw nut.

When the clutch is engaged, the ball screw input torque drives the generator to rotate and generate electricity. Taking the PTO system and the generator as the research object, the dynamic

equation can be expressed as shown in Equation (12).

$$T_s - T_g = J\alpha \tag{12}$$

where, T_g is the generator torque, J is the equivalent moment of inertia of the PTO system and the generator, α is the angular acceleration.

The generator torque T_g can be regarded as an expression proportional to the generator speed:

$$T_g = \frac{K_t K_e}{(R_i + R_e)} \omega_g \tag{13}$$

where K_t is the torque constant, K_e is the electrical constant, R_i is the internal resistance of the generator, R_e is the external load resistance of the generator, and ω_g is the angular velocity of the generator.

Because the transmission ratio between the bevel gears is 1, the generator speed and the ball screw speed are equal, that is, $\omega_g = \omega_s$ and $\alpha = \dot{\omega}_s$. Combining Equations (12) and (13) can be obtained:

$$T_s = J\omega_s + \frac{K_t K_e}{(R_i + R_e)}\omega_s \tag{14}$$

Incorporating Equations (9) and (11) into Equation (14), the system PTO force can be obtained as:

$$F_{pto} = J\frac{4\pi^2}{l^2\eta_s}\ddot{z} + \frac{4\pi^2}{l^2\eta_s}\frac{K_t K_e}{(R_i + R_e)}\dot{z} \tag{15}$$

Suppose the equivalent mass m_e' and damping coefficient c_e' of the PTO system are respectively:

$$m_e' = J\frac{4\pi^2}{l^2\eta_s}, \quad c_e' = \frac{K_t K_e}{(R_i + R_e)}\frac{4\pi^2}{l^2\eta_s} \tag{16}$$

Then the PTO force can be expressed as:

$$F_{pto} = m_e'\ddot{z} + c_e'\dot{z} \tag{17}$$

When the clutch is in the disengaged state, the PTO system will be dissociated into two sub-systems, one is the no-load subsystem driven by the ball screw. The other is the self-powered subsystem driven by the potential energy stored in the moment of inertia of the generator mover. The Equation (14) can be expressed as:

$$J\omega_g + \frac{K_t K_e}{(R_i + R_e)}\omega_g = 0 \tag{18}$$

Through Equation (18), the generator speed at this time can be calculated as:

$$\omega_g = e^{kt}, k = -\frac{K_t K_e}{(R_i + R_e)J} \tag{19}$$

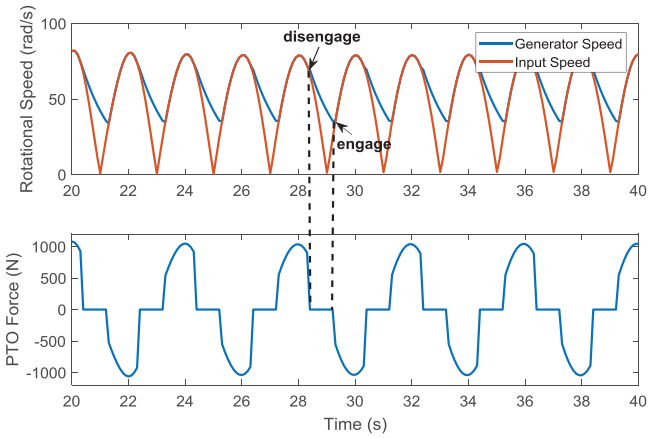

FIGURE 6 Generator speed and PTO force in engaged and disengaged states

The results show that the generator speed will decrease exponentially during separation.

When the clutch is in the engaged state, its motion response equation is:

$$\begin{cases} \left(m + m_a + m_e'\right)\ddot{z}(t) + \left(c_{rt} + c_e'\right)\dot{z}(t) + \rho g A z(t) = F_{et} \\ \omega_g = \omega_s = \dfrac{2\pi}{l}\dot{z}(t) \end{cases} \tag{20}$$

When the clutch is in the disengaged state, its motion response equation is:

$$\begin{cases} (m + m_a)\ddot{z}(t) + c_{rt}\dot{z}(t) + \rho g A z(t) = F_{et} \\ J\omega_g + \dfrac{K_t K_e}{(R_i + R_e)}\omega_g = 0 \end{cases} \tag{21}$$

According to the mathematical model, the dynamic simulation analysis result under sine wave excitation is shown in Figure 6.

3.3 | Dynamic model and simulation of the permanent magnet synchronous generator

When modelling the permanent magnet synchronous generators, the following assumptions should be made: The stator three-phase winding is completely symmetrical, and its induced electromotive force is a three-phase symmetrical sine wave; Ignore eddy current and hysteresis loss; Ignore the damping winding of the generator mover; the influence of temperature on generator parameters is not considered [23, 24].

When the generator is working, the generator rotor cuts the magnetic lines of induction to generate induced electromotive force. The induced electromotive force can be expressed as

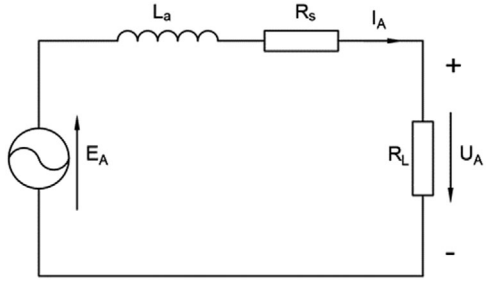

FIGURE 7 The single-phase equivalent circuit of a permanent magnet synchronous generator

shown in Equation (22).

$$\begin{cases} E_A = \dfrac{d\psi_A}{dt} = -\omega\psi_f \sin\theta \\ E_B = \dfrac{d\psi_B}{dt} = -\omega\psi_f \left(\sin\theta - 2\pi/3\right) \\ E_C = \dfrac{d\psi_C}{dt} = -\omega\psi_f \left(\sin\theta + 2\pi/3\right) \end{cases} \tag{22}$$

where E_A, E_B and E_C are the three-phase induced electromotive force, ψ_A, ψ_B, ψ_C are the flux linkage of the three-phase winding, ω is the rotor electrical angular velocity, ψ_f is the permanent magnet flux linkage, and θ is the electrical angle between the rotor flux linkage and the winding axis.

The single-phase equivalent circuit of a permanent magnet synchronous generator is shown in Figure 7.

Taking phase A as an example, according to Kirchhoff's voltage law, the single-phase voltage equation of the generator can be obtained as shown in Equation (23).

$$E_A = L_A \frac{di_A}{dt} + i_A \left(R_s + R_L\right) = L_A \frac{di_A}{dt} + i_A R_s + U_A \tag{23}$$

where, E_A is the A-phase induced voltage, L_A is the A-phase inductance, i_A is the A-phase current, R_s is the stator internal resistance, R_L is the A-phase load resistance, and U_A is the output voltage at the load.

Combining Equations (22) and (23) can get the generator stator terminal voltage equation as shown in Equation (24).

$$\begin{cases} U_A = -i_A R_s - L_A \dfrac{di_A}{dt} + \dfrac{d\psi_A}{dt} \\ U_B = -i_B R_s - L_B \dfrac{di_B}{dt} + \dfrac{d\psi_B}{dt} \\ U_C = -i_C R_s - L_C \dfrac{di_C}{dt} + \dfrac{d\psi_C}{dt} \end{cases} \tag{24}$$

The single-phase output power of the generator is shown in Equation (25).

$$P_{out} = \frac{V^2}{R_L} \tag{25}$$

where, P_{out} is the generator single-phase output power, V is the generator single-phase output voltage, R_L is the single phase load resistance.

The transformation equation of the voltage from the three-phase stationary coordinate system to the two-phase rotating coordinate system is shown in Equation (26).

$$\begin{bmatrix} u_d \\ u_q \end{bmatrix} = \frac{2}{3} \begin{bmatrix} \cos\theta & \cos\left(\theta - \frac{2\pi}{3}\right) & \cos\left(\theta + \frac{2\pi}{3}\right) \\ -\sin\theta & -\sin\left(\theta - \frac{2\pi}{3}\right) & -\sin\left(\theta + \frac{2\pi}{3}\right) \end{bmatrix} \begin{bmatrix} u_A \\ u_B \\ u_C \end{bmatrix} \tag{26}$$

According to Equations (25) and (26), the voltage equation in the dq coordinate system can be calculated as:

$$\begin{cases} u_d = -R_s i_d - \omega_e L_q i_q + L_d \dfrac{di_d}{dt} \\ u_q = -R_s i_q - \omega_e L_d i_d + L_q \dfrac{di_q}{dt} + \omega\psi_f \end{cases} \tag{27}$$

where, i_d and i_q are the components of the stator winding current on the d shaft and q shaft respectively, L_d and L_q are the components of the stator inductance on the d shaft and q shaft respectively, and ω_e is the electrical angular velocity of the rotor.

The electromagnetic torque equation of the generator in the dq coordinate system can be expressed as:

$$T_g = \frac{3}{2} n_p \left[\psi_f i_q + \left(L_d - L_q\right) i_d i_q\right] \tag{28}$$

According to the mathematical modelling of the permanent magnet synchronous generator, the simulation model is built in Matlab/Simulink. According to the simulation model and various parameters of the generator, the single-phase voltage, current and power at the output of the generator under given sea conditions can be obtained. Taking phase A as an example, the output single-phase voltage, current and power are shown in Figure 8.

It can be seen that the period of single-phase voltage, current and power is 2 s, and its frequency is twice the wave frequency. The single-phase voltage amplitude is about 50 V, the current amplitude is about 2 A, and the power amplitude is about 120 W. Since the system input is a regular wave, its voltage, current and power waveforms all change sinusoidally.

According to the single-phase instantaneous output power calculation Equation (25), the three-phase average total electric power output by the generator in a period of time T can be obtained as:

$$P_{ave} = 3 \times \frac{\int_0^T P_{out}\, dt}{T} \tag{29}$$

When the wave period is 4 s, the wave height is 0.4 m, and the load resistance is 23 **Ω**, the average electric power output by the generator is shown in Figure 9. It shows that the average

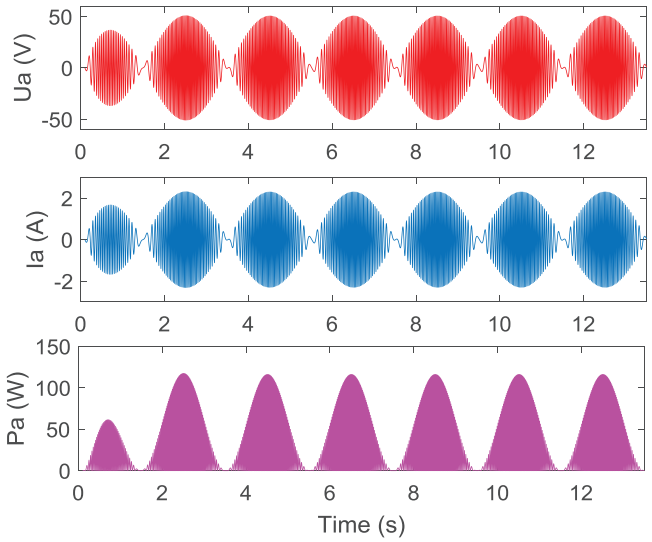

FIGURE 8 Generator single-phase voltage, current and power

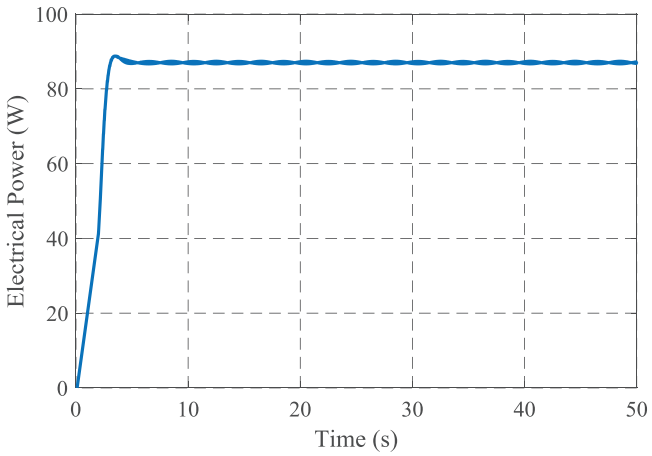

FIGURE 9 Average electric power output by generator

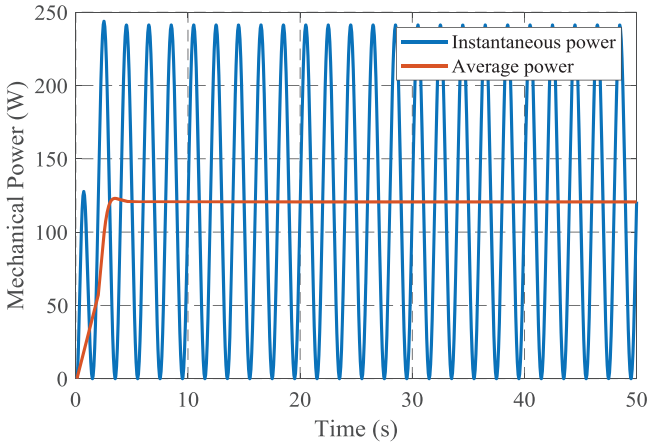

FIGURE 10 Input mechanical power

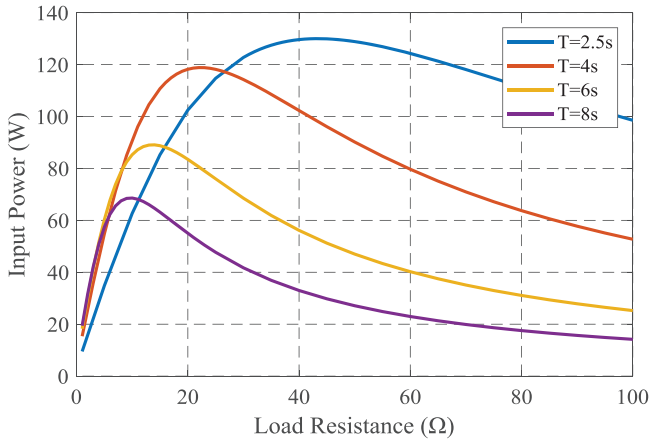

FIGURE 11 Input power varies with load resistance under different wave period

electric power output by the generator is about 85.77 W after stabilization.

In addition to the output power of the generator, the mechanical power input to the system should also be considered, it can be expressed as shown in Equation (30).

$$P_{in} = F_{pto}\,\dot{\chi} \tag{30}$$

The mechanical power input to the PTO system under the same wave conditions and load resistance is shown in Figure 10. It can be seen from the figure that the average mechanical power input is about 118.85 W after stabilization.

The power generation efficiency of the PTO system is the ratio of electrical power to mechanical power, and it can be expressed as shown in Equation (31).

$$\eta = \frac{P_{out}}{P_{in}} \tag{31}$$

According to Equation (31), the power generation efficiency of the PTO system is 0.72 when the load resistance is 23 Ω.

For the WEC, its damping coefficient is mainly related to the load resistance of the generator. Therefore, the damping coefficient of the PTO system can be changed by adjusting the load resistance of the generator, so as to achieve the maximum power capture of the wave energy power generation system.

According to the mathematical model of the generator and the calculated hydrodynamic parameters. By establishing a simulation model in Simulink, we can get the curve of input and output power versus load resistance under different wave periods, as shown in Figures 11 and 12.

It can be seen from the Figures 11 and 12 that the input and output power changes in the same trend with the load resistance. The smaller the wave period, the greater the energy density, and the greater the maximum power obtained. At the same time, the load resistance at the maximum power point is also related to the wave period. Therefore, when the wave period changes, the load resistance at the maximum power will also change. It can be seen from Table 1 that the larger the wave period, the smaller the load resistance at the maximum power point.

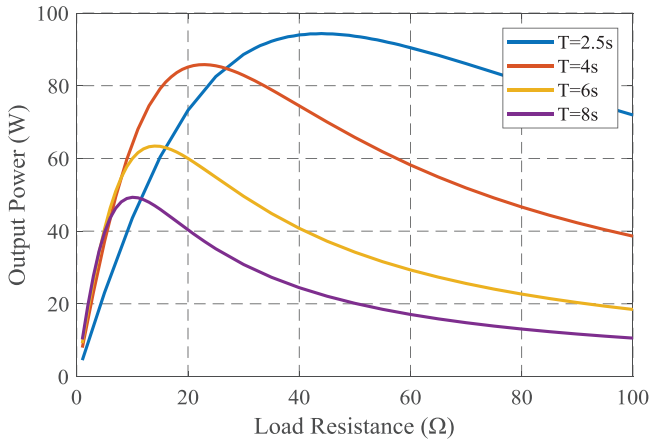

FIGURE 12 The output power varies with load resistance under different wave period

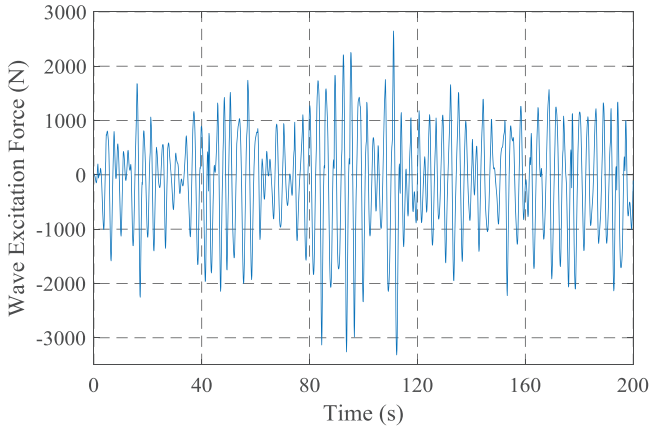

FIGURE 13 Wave excitation force under random wave conditions with a spectral peak period of 3 s and a significant wave height of 0.4 m

TABLE 1 Maximum input and output power under different wave periods

Wave period T(s)	Maximum input power P_{in} (W)	Maximum output power P_{out} (W)	Load resistance at maximum power (Ω)
2.5	129.99	94.36	44
4	118.85	85.82	23
6	89.08	63.4	14
8	68.59	49.31	10

By analyzing the change of input and output power with load resistance under different wave periods, it can be known that there is an optimal load resistance under different wave conditions to maximize the power generation. That is, there is an optimal damping in the PTO system, and the power generation efficiency can be improved by searching for the optimal damping.

3.4 | Analysis of obtaining optimal power under random waves

The previous analysis of the WEC are all carried out on the basis of regular waves. However, the actual ocean waves are constantly changing and are composed of a variety of waves with different wave heights and frequencies. Therefore, we need to analyse the optimal power acquisition under random waves to make it more in line with the actual marine environment.

Ocean waves are a relatively complicated random process. At present, ocean waves are mainly described in the form of ocean wave spectrum [25]. So far, many wave spectra have been proposed, the general expression can be shown in Equation (32).

$$S(\omega) = \frac{A}{\omega^p} exp\left(-B\frac{1}{\omega^q}\right) \tag{32}$$

where $S(\omega)$ is the distribution of wave energy relative to its component frequency, the index p is often 4–6, the index q is often 2–4, A and B contains wind element or wave element as a parameter.

At present, the most widely used wave spectra are mainly PM spectrum and JONSWAP spectrum [26]. Because the latter takes into account the influence of wind speed and wind distance, it can better reflect the real situation of the waves. In this paper, JONSWAP spectrum is used to model random waves, and its expression can be shown in Equation (33).

$$S(\omega) = \alpha g^2 \frac{1}{\omega^5} \exp\left[-\frac{5}{4}\left(\frac{\omega_m}{\omega}\right)^4\right] \gamma^{\exp\left[-\frac{(\omega-\omega_m)^2}{2\sigma^2\omega_m^2}\right]} \tag{33}$$

where α is the energy scale parameter, ω is the angular frequency of the wave, ω_m is the peak frequency, γ is the peak elevation factor, and σ is the peak shape parameter.

The random wave excitation force generated by the JONSWAP spectrum with a peak period of 3 s and a significant wave height of 0.4 m is shown in Figure 13.

Using Simulink software for simulation, the input and output power under random wave conditions with a spectral peak period of 3 s and a significant wave height of 0.4 m can be obtained, as shown in Figures 14 and 15.

It can be seen from Figure 14 that the instantaneous power fluctuates greatly, which is closer to the actual power generation under sea conditions. By integrating the instantaneous power and calculating its average value, it will probably stabilize at 200 s. When the load resistance is 23 Ω, the average output power is 54.57 W.

It can be seen from Figure 15 that the input mechanical power is similar to the output electrical power curve, the power fluctuation is relatively large, and the average value is calculated after integration. After stabilization, the average input power is 75.62 W, and the efficiency is about 0.72. Since the load resistance is 23 Ω during the simulation, the efficiency under random waves is the same as the efficiency under regular waves.

By modelling the random wave, we can get the curve of input and output power versus load resistance under different random

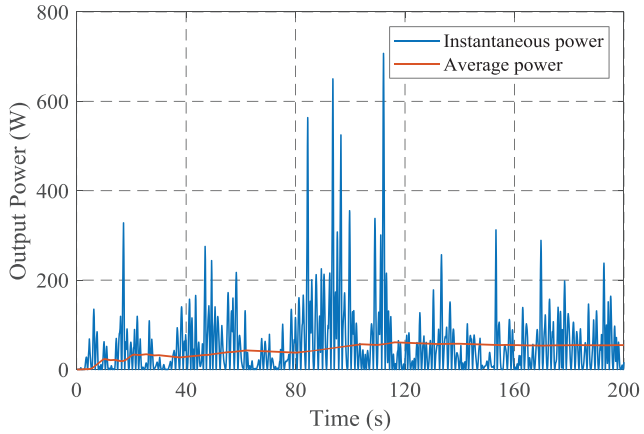

FIGURE 14 Output power under random wave conditions with a spectral peak period of 3 s and a significant wave height of 0.4 m

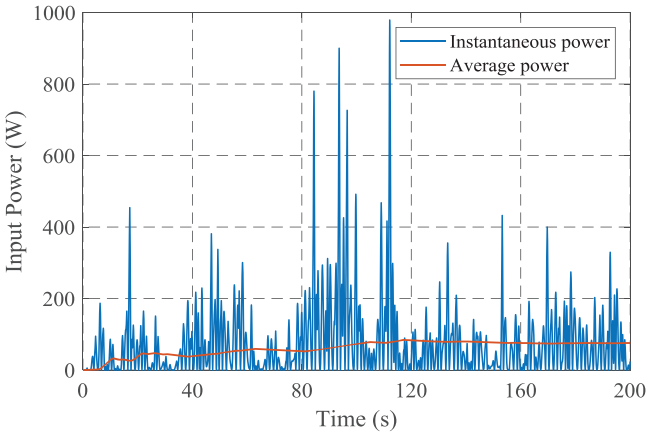

FIGURE 15 Input power under random wave conditions with a peak period of 3 s and a significant wave height of 0.4 m

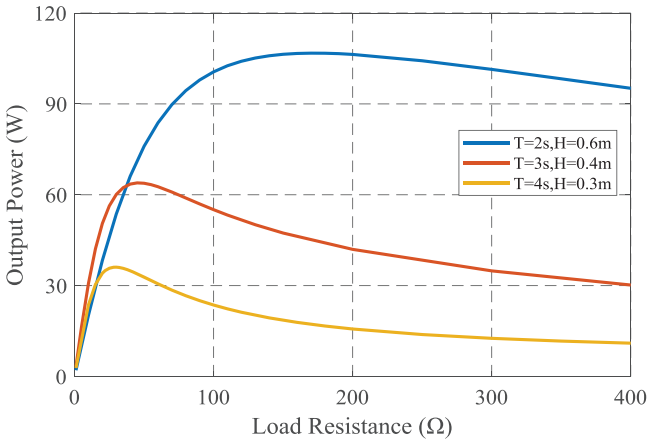

FIGURE 16 The output power varies with load under different wave conditions

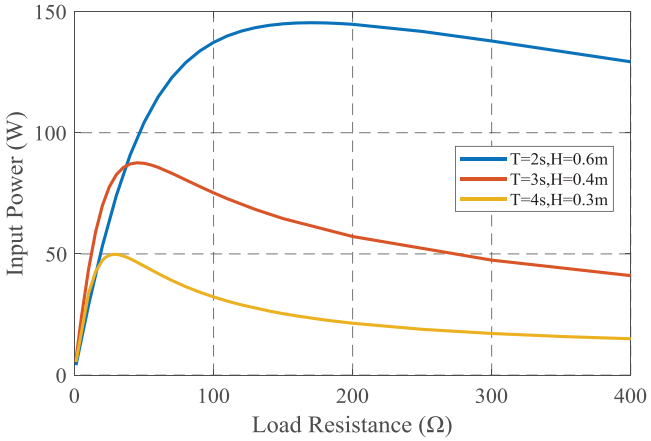

FIGURE 17 Input power varies with load under different wave conditions

wave conditions, as shown in Figures 16 and 17. The wave peak periods are 2, 3, 4 s, and the significant wave heights are 0.6, 0.4, 0.3 m.

It can be seen from the Figure 16 that the output power change curve with load under random waves is roughly the same as that under regular waves. As the load resistance increases, the output power first increases and then decreases. There is an optimal load resistance corresponding to the maximum power point. And the smaller the wave period, the larger the corresponding load resistance at the maximum power point.

The curve of input power versus load resistance under different wave conditions is shown in Figure 17. The change trend is the same as that of output power. There is an optimal load resistance corresponding to the maximum input power under each sea condition.

It can be seen from Figures 16 and 17 that the optimal damping theory is also met under random wave conditions, and the maximum power point can also be found by adjusting the load resistance of the generator, thereby improving power generation efficiency.

Therefore, the optimal power acquisition analysis lays the foundation for the MPPT algorithm. We can find the maximum power point under current sea conditions through the maximum power point tracking algorithm.

4 | MAXIMUM POWER POINT TRACKING ALGORITHM

4.1 | Design of maximum power point tracking algorithm

Through the analysis of the optimal power acquisition of WEC, the curve of power generation versus load resistance under different wave conditions is obtained. The optimal damping theory is verified, that is, there is an optimal damping coefficient corresponding to the maximum power point in each wave condition.

Due to the load resistance is fixed under actual conditions, a Buck-Boost circuit is added to the generator output. By changing the duty cycle of the switch tube in the circuit, the variable load adjustment is realized, thereby realizing the

maximum power under different wave conditions. The relationship between the input and output load resistances in the Buck-Boost circuit is shown in Equation (34).

$$R_{in} = \left(\frac{1-D}{D}\right)^2 R_L \tag{34}$$

In order to enable the PTO system automatically output the maximum power, a control algorithm needs to be adopted to make the wave energy power generation system have a self-optimizing function. At present, the maximum power point tracking control is mostly used in photovoltaic power generation and wind power generation. As an adaptive control method, it can also be used in wave energy power generation system. This paper is based on the admittance differentiation method to design the maximum power point tracking algorithm. First sample the voltage and current, calculate the output power, and then apply a disturbance to the system. By comparing the output power before and after the disturbance, we can judge whether the direction of the disturbance is correct. If the output power increases, continue to apply the disturbance in this direction. Because the step length of the admittance differentiation method is set to a value proportional to the slope of the power curve, the power will continuously approach and finally stabilize at the maximum power point by continuously applying disturbances, thereby achieving the tracking of the maximum power point.

The flow of the maximum power point tracking algorithm designed in this paper is shown in Figure 18. It mainly includes four parts: the setting of the initial conditions, the power calculation, the judgment of the disturbance direction, and the setting of the step length. The setting range of the initial duty cycle is 0–1, and the initial disturbance direction is set according to the value of the initial duty cycle. When the initial duty cycle is set relatively large, the initial disturbance direction is set to −1. When the initial duty cycle setting is relatively small, the initial disturbance direction is set to 1. The sampling period should also be set reasonably. For regular waves, the wave input energy changes periodically, and the output power also changes periodically. Therefore, it is generally set to an integer multiple of the wave period. For random waves, the wave input does not have regularity in the short term, but the wave input energy can also be considered relatively stable from a larger dimension. Therefore, for random waves, the sampling period should be increased. The setting of the step length is the focus of the algorithm. When the power change is greater than 20 W, the step length is set to 0.03. In other cases, the step value is set to a value proportional to the slope of the power curve, α is a coefficient value, which is set as 0.005 in this paper.

For random waves, due to large fluctuations in input energy, the output power fluctuation after averaging is still relatively large, and the algorithm is difficult to operate stably. Therefore, this paper adds two low-pass filters to filter the average output power, which makes the output power more stable and facilitates the control of the algorithm.

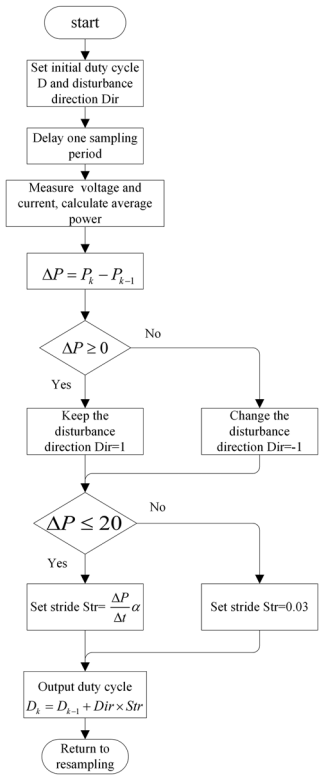

FIGURE 18 Maximum power point tracking algorithm flowchart

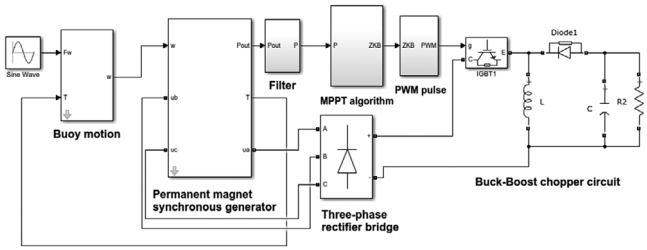

FIGURE 19 Simulink simulation model

4.2 | Simulation results

In this section, a simulation model is established in Simulink, and the algorithm is simulated to verify its correctness. The simulation model of the algorithm is shown in Figure 19. After the generator output voltage is rectified through the three-phase rectifier bridge, it is used as the input of the Buck-Boost chopper circuit. The electric power output by the generator is averaged and filtered as the input of the maximum power point tracking algorithm. The algorithm finally outputs the corresponding duty cycle at the maximum power point. The pulse signal is generated by the PWM pulse generator to control the on-time of the switch in the Buck-Boost circuit, so as to realize the adjustment of the load resistance, and finally realize the maximum power point tracking control.

According to the above simulation model, set the wave condition as 4 s period, 0.4 m wave height, initial duty cycle 0.35, and initial disturbance direction 1. The simulation results of the

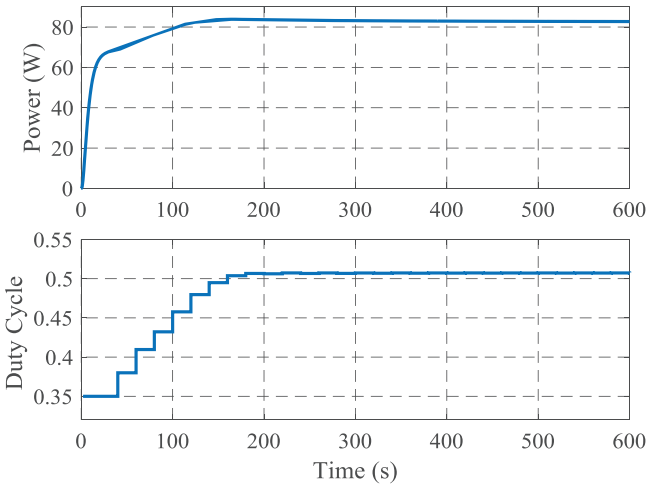

FIGURE 20 Simulation results of the algorithm for regular waves with a wave period of 4 s and a wave height of 0.4 m

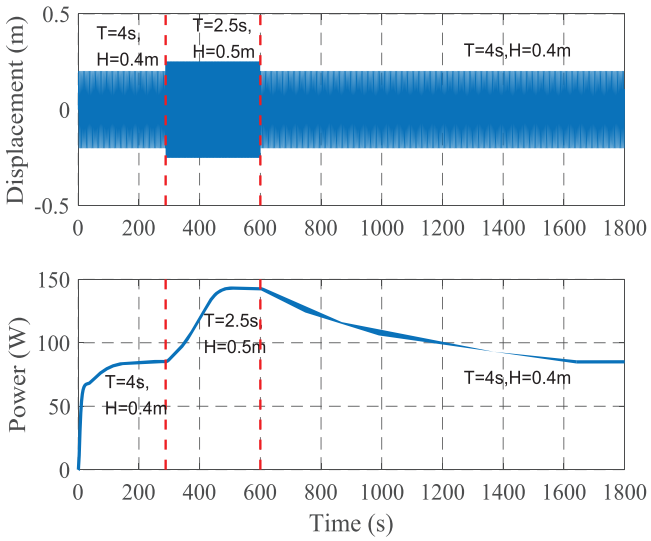

FIGURE 21 Simulation results of the algorithm under changing regular wave conditions

algorithm under regular wave conditions with a period of 4 s and a wave height of 0.4 m are shown in Figure 20.

It can be seen from Figure 20 that the maximum power obtained by the algorithm is 82.5 W, and the duty cycle at the maximum power is 0.506. According to the Equation (34), the load resistance value corresponding to the duty cycle of 0.506 is 23.83 Ω. The maximum output power under wave condition with a period of 4 s and a wave height of 0.4 m obtained by simulation is 85.82 W, which is only 3.32 W away from the power obtained by the maximum power point tracking algorithm. The load resistance at the maximum power obtained by the simulation is 23 Ω. The difference between them is only 0.83 Ω. It can be seen that the difference between the maximum power obtained by the algorithm and the maximum power obtained by multiple simulations is very small, which verifies the correctness of the algorithm.

In order to further verify the feasibility of the algorithm, a variable sea state analysis was performed on the basis of the regular wave period of 4 s and the wave height of 0.4 m. The simulation result is shown in Figure 21.

It can be seen from the Figure 21 that the initial wave condition is 4 s period and 0.4 m wave height, and reach the maximum power point at about 200 s, and the power generation is stable at 82.5 W. At 288 s, the wave condition is changed to a period of 2.5 s and a wave height of 0.5 m. After that, the maximum power point under the current wave condition was found at about 500 s and reached a steady state. At 600 s, the wave condition is changed again to a period of 4 s and a wave height of 0.4 m, and the maximum power point under the current wave condition is found again at about 1600 s. The feasibility of the algorithm is verified by the simulation analysis of the algorithm under changing sea conditions.

From the simulation results in Section 3.4, it can be seen that there is also a maximum power point under random wave conditions. Therefore, it is necessary to verify the feasibility of the algorithm under random wave conditions. Set the random wave

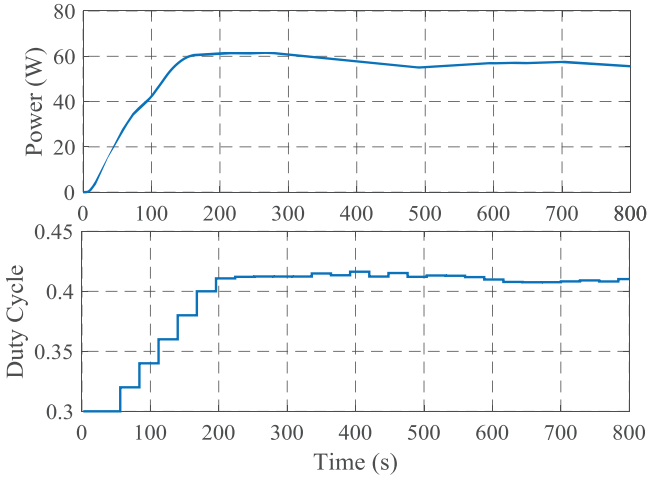

FIGURE 22 Simulation results of the algorithm for random waves with a wave period of 3 s and a wave height of 0.4 m

condition as the peak period of 3 s and the significant wave height of 0.4 m. The simulation result is shown in Figure 22.

It can be seen from the Figure 22 that the algorithm finds that the maximum power is 61.4 W at about 200 s, and the duty cycle at the maximum power is 0.415. According to the Equation (34), the load resistance corresponding to the duty cycle of 0.415 is 49.68 Ω. The maximum power obtained through simulation in Section 3.4 is 63.81 W, the corresponding load resistance is 50 Ω, the maximum power difference is 2.41 W, and the load resistance difference is 0.32 Ω, which is a small difference. Therefore, by increasing the sampling period and filtering the average output power, the algorithm can still find the maximum power point under random wave conditions.

Similarly, the variable sea condition analysis is performed on the basis of the random wave spectrum peak period 3 s and the significant wave height 0.4 m. The simulation result is shown in Figure 23.

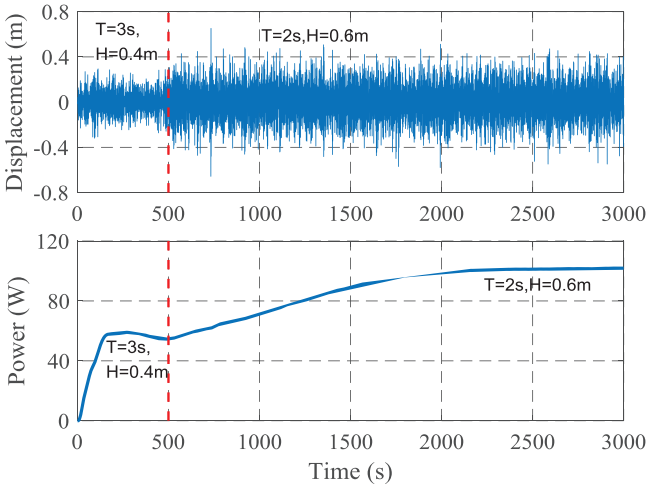

FIGURE 23 Simulation results of the algorithm under changing random wave conditions

It can be seen from the Figure 23 that the initial wave condition is the peak period of 3 s and the significant wave height of 0.4 m. The algorithm finds the maximum power point at about 200 s, and then the power stabilizes at 61.4 W. At 500 s, the wave condition was changed to the peak period of 2 s and the significant wave height of 0.6 m. After that, the maximum power point under the current sea condition was found again at about 2000 s and reached a steady state. Through simulation analysis under random wave changing sea conditions, the feasibility of the algorithm under random wave conditions is verified.

5 | CONCLUSION

This paper mainly designs a mechanical rectification wave energy converter, which uses the ball screw to efficiently convert low-speed linear motion into high-speed rotary motion, and uses a ball screw mechanism to convert energy. The buoy and the screw nut are coupled together by a magnetic coupling force transmission system, which solves the sealing problem in the water, and adopts a mechanical rectification mechanism to convert the two-way rotating motion of the screw into a continuous one-way rotating motion, ensuring the normal service life of the generator.

Based on the airy wave theory, the wave force of the buoy is analysed in the frequency domain. The wave excitation force, add mass and radiation damping of the buoy are obtained through ANSYS/AQWA software. Based on the hydrodynamic parameters of the buoy, a mathematical model of linear PTO is established, and the displacement, PTO force and power of the buoy when the damping coefficient is 4000 N/(m/s) are obtained through simulation.

The permanent magnet synchronous generator is modelled and have a simulation analysis. The simulation analysis shows that when the wave period is 4 s, the wave height is 0.4 m, and the load resistance is 23 Ω, the input and output power of the power generation system are 118.85 and 85.77 W. Its power generation efficiency is 0.72.

Under regular wave conditions, by adjusting the load resistance of the generator, the relationship between power and load resistance is obtained, which verifies the optimal damping theory, that is, there is an optimal system damping corresponding to the maximum power. In order to simulate the actual ocean wave conditions, the simulation model of random waves is established, the relationship between power and load resistance under random waves is obtained, and the optimal damping theory under random wave conditions is verified.

In order to improve power generation efficiency, based on the optimal damping theory under different wave conditions, the maximum power point tracking algorithm is designed. The Buck-Boost chopper circuit is added to the output of the generator, and the variable load regulation is realized by changing the duty ratio of the switch in the circuit. In view of the disturbance error in the traditional disturbance observation method, this paper adopts the admittance differentiation method to design the maximum power point tracking algorithm. By setting the step length to a value proportional to the power curve, the disturbance error is reduced, and two low-pass filters are added to filter the average power, so that the algorithm is equally applicable under random wave conditions. The simulation results of the algorithm are compared with the maximum power point obtained by multiple simulations, and the feasibility and correctness of the algorithm are verified. Therefore, the tracking control of the maximum power point is realized.

REFERENCES

1. Melikoglu, M.: Current status and future of ocean energy sources: A global review. Ocean Eng. 148, 563–573 (2018)
2. Falco, A.F.O: Wave energy utilization: A review of the technologies. Renewable Sustainable Energy Rev. 14(3), 899–918 (2010)
3. Wang R, Q., Ning D, Z.: Dynamic analysis of wave action on an OWC wave energy converter under the influence of viscosity. Renewable Energy 150, 578–588 (2020)
4. M'Zoughi, F., et al.: Self-adaptive global-best harmony search algorithm-based airflow control of a wells-turbine-based oscillating-water column. Appl. Sci. 10(13), 28–46 (2020)
5. Ansarifard, N., et al.: Design optimisation of a unidirectional centrifugal radial-air-turbine for application in OWC. Wave Energy Converters. Energies 12(2791), 267–277 (2019)
6. Parmeggiani, S., et al.: Modelling of the overtopping flow on the wave dragon wave energy coverter. ICOE 2011(2011), 443–636 (2010)
7. Prado, M.: Case study of the Archimedes Wave Swing (AWS) direct drive wave energy pilot plant. Electr. Drives Direct Drive Renewable Energy Syst. 195(2), 195–218 (2013)
8. Gao, Y., et al.: A fully floating system for a wave energy converter with direct-driven linear generator. Energy 95(jan.15), 99–109 (2016)
9. Carrelhas, A.A.D., et al.: Test results of a 30kW self-rectifying biradial air turbine-generator prototype. Renewable Sustainable Energy Rev. 109(JUL), 187–198 (2019)
10. Agamloh, E.B., Wallace, A.K., Jouanne, A.V.: A novel direct-drive ocean wave energy extraction concept with contact-less force transmission system. Renewable Energy 33(3), 520–529 (2008)
11. Martin, D., et al.: Numerical analysis and wave tank validation on the optimal design of a two-body wave energy converter. Renewable Energy 145(Jan), 632–641 (2020)
12. Nebel, P.:. Maximizing the efficiency of wave-energy plant using complex-conjugate control. Proc. Inst. Mech. Eng. 206(4), 225-236 (2016)
13. Hardy, P., et al.: A maximum capture width tracking controller for ocean wave energy converters in irregular waves. Ocean Eng. 121(JUL.15), 516–529 (2016)

14. Giorgi, G., Ringwood, J.V.:. Implementation of latching control in a numerical wave tank with regular waves. J. Ocean Eng. Marine Energy 2(2), 211–226 (2016)
15. Mon, B.F., et al.: Adaptive maximum power point tracking algorithm for heaving wave energy converters. In: OCEANS, Marseille, pp. 1–5 (2019)
16. Brekken, T.K.A: On model predictive control for a point absorber wave energy converter. In: IEEE Trondheim PowerTech, Trondheim, Norway, pp. 1–8 (2011)
17. Xiao, X., Huang, X., Kang, Q.: A hill-climbing-method-based maximum-power-point-tracking strategy for direct-drive wave energy converters. IEEE Trans. Ind. Electron. 63(1), 257–267 (2015)
18. Ding, B., et al.: Sea-state based maximum power point tracking damping control of a fully submerged oscillating buoy. Ocean Eng. 126, 299–312 (2016)
19. Amon E.A., Brekken, T.K.A., Schacher, A.A.: Maximum power point tracking for ocean wave energy conversion. IEEE Trans. Ind. Appl. 48(3), 1079–1086 (2012)
20. Rajaei, A.H., et al.: PMSG-based variable speed wind energy conversion system using Vienna rectifier. Int. Trans. Electr. Energy Syst. 21(1), 954–972 (2013)
21. Danandeh, M.A., Mousavi, G.S.M: Comparative and comprehensive review of maximum power point tracking methods for PV cells. Renewable Sustainable Energy Rev. 82(PT.3), 2743–2767 (2018)
22. Falnes, J., Ocean Waves and Oscillating Systems. Cambridge University Press, Cambridge (2002)
23. Nie, Z., et al.: Emulation and control methods for direct drive linear wave energy converters. IEEE Trans. Ind. Inf. 9(2), 790–798 (2013)
24. Polinder, H., Damen, M.E.C., Gardner, F.: Design, modelling and test results of the AWS PM linear generator. Int. Trans. Electr. Energy Syst. 15(3), 245–256 (2013)
25. Amurol, S., Ewans, K.: The effect of swell on wave spectra of extreme sea states offshore Sarawak. Ocean Eng. 189, 106–288 (2019)
26. Ji, X., et al.: Modelling of linear and non-linear two-body wave energy converters under regular and irregular wave conditions. Renewable Energy 147, 487–501 (2020)

How to cite this article: Xu Jianan, et al.: Maximum power point tracking control for mechanical rectification wave energy converter. IET Renew. Power Gener. 15:3138–3150 (2021).
https://doi.org/10.1049/rpg2.12213.